

Defect development in a three-dimensional reaction-diffusion system with gradient

Chunyan Wang,¹ Xiaochuan Lu,¹ Huimin Liao,¹ Qi Ouyang,^{1,2,3,*} and Hongli Wang^{1,2,3,†}

¹State Key Laboratory for Mesoscopic Physics, Department of Physics, Peking University, Beijing 100871, China

²Center for Theoretical Biology, Peking University, Beijing 100871, China

³The Beijing-Hong Kong-Singapore Joint Center for Nonlinear and Complex Systems (PKU), Beijing 100871, China

(Received 10 July 2008; published 9 February 2009)

The formation and development of spiral defects is one of the major causes of order-disorder transitions in spatiotemporal patterns. In this paper, line defect formation and development in a three-dimensional reaction-diffusion system with gradients of control parameters in the third dimension is investigated. The system can be considered as diffusively coupled two-dimensional spatiotemporal patterns with dissimilarities. We observed that under certain conditions, as the gradients are varied, ordered and disordered spatiotemporal patterns appear alternately and line defects of various configurations form. This scenario is found to be in qualitative agreement with the experimental findings in the Belousov-Zhabotinsky reaction. We thus demonstrate that the line defect which was usually expected in two-dimensional complex oscillatory media can also be generated from the reconciliation between the coupled simple spiral waves with dissimilarity.

DOI: [10.1103/PhysRevE.79.026207](https://doi.org/10.1103/PhysRevE.79.026207)

PACS number(s): 82.40.Ck, 47.20.Ky, 47.54.-r

I. INTRODUCTION

Collective behaviors of a population of coupled entities with dissimilarity are ubiquitous in the natural world. Coherent synchronization in which a system of interacting oscillators with a frequency difference spontaneously locks into a common frequency has been found to be important in many processes, such as in biology [1–4], physics [5], chemistry [6], and engineering [7]. Since the pioneering works of Wiener [8], Winfree [9], and Kuramoto [10], collective behavior in populations of interacting oscillators has been the topic of intensive investigations [11]. More recent research has been now extended to more general dynamics such as mixed collections of chaotic oscillators or maps [12], and to more general interaction networks with complex topology [13].

In this paper, we consider a special coupled system, a train of spirals diffusively coupled in a one-dimensional chain. The system is distinctive in that the interacting entities are spatiotemporal patterns rather than temporal limit-cycle oscillators, and our system is diffusively coupled rather than the style of coupling of discrete oscillators. This coupled system can be experimentally realized [15] with the spatial open reactor where reactants have gradients across the thin porous glass disk and can be modeled with three-dimensional (3D) reaction-diffusion kinetics with gradients in the third direction [16]. Due to the gradients, the coupled spirals are slightly different in their properties.

It has been documented that a homogeneous 3D reaction-diffusion system supports scroll waves; a well-known mechanism of instability called “negative tension instability” can render the scroll waves to lose their stability and undergo a transition to spatiotemporal turbulence or “Winfree turbulence” [17–20]. A scenario for taming “Winfree turbulence” was also proposed [21]. In a 3D system with parameter gra-

dients, experiments with the Belousov-Zhabotinsky (BZ) reaction and numerical simulations with the Fitzhugh-Nagumo model [16] revealed that, when the system is in the oscillatory regime and the coupling strength is weak, a scroll wave ring can spontaneously form. This ring of scroll wave can lose its stability when the gradient of control parameters are increased. The control of this type of spiral turbulence was recently discussed [22,23].

When the 3D system with gradient is in or near the excitable regime and the coupling strength becomes stronger, the system may behave very differently. For example, Yoneyama *et al.* observed spiral waves with a line defect with the BZ reaction in a petri dish over a decade ago [24]. In spatial open reactors, line-defected spiral waves and turbulence have been investigated extensively in experiments of the BZ reaction by Lee’s group [25–27] and ours [14,15]. On the theoretical side, Kapral and his collaborators [28–30] proved that the line defect is a two-dimensional effect and is the consequence of period-doubling of the local dynamics. The purpose of this paper is to illustrate that the line defect observed in the 3D spatial open reactor can be a consequence of the coupling and reconciliation of two-dimensional patterns with dissimilarity, which is a different interpretation from the currently accepted scenario of period-doubling.

Using the Oregonator model, we show that as the dissimilarities in spirals are increased by tuning the gradients, the system may split into two parts: one retains an ordered spiral regime, the other turns into turbulence. The alternate appearance of ordered and disordered states is observed as the gradients are increased. During the process, dynamical line defects evolve out of turbulence as the reconciliation between the dissimilar spirals and dominate the second-time transition to turbulence. The line defects we observed in the simulation are qualitatively consistent with the experimental findings in the BZ reaction.

II. SIMULATION MODEL

We consider the Oregonator for the BZ reaction [31] in 3D space with gradients of the control parameter in the third

*Corresponding author. qi@pku.edu.cn

†Corresponding author. hlwang@pku.edu.cn

dimension. Following Ref. [32], we use the model that adopts Vastano's scaling, which is given by the following equations:

$$\frac{\partial u}{\partial \tau} = \frac{1}{\varepsilon} \left(Au - u^2 + fBv \frac{qA - u}{qA + u} \right) + D_u \nabla^2 u, \quad (1a)$$

$$\frac{\partial v}{\partial \tau} = Au - Bv + D_v \nabla^2 v. \quad (1b)$$

The variable u corresponds to the concentration of the bromous acid and v to the concentration of the oxidized form of the metal ion catalyst. The coefficient q is a combination of rate constants of the three-variable Oregonator, and f is stoichiometric factor. The kinetic equations also include bromate (labeled A) and the organic substrate (labeled B).

We assume that only the reaction and diffusion processes take place in a 3D space with multiple gradients in a third thin direction, and perform numerical integrations of Eqs. (1a) and (1b). Our simulations are carried out in the Cartesian coordinate system with a grid size of $256 \times 256 \times 15$ and a uniform spatial step $h=0.01$. The system consists thus of 15 diffusively coupled layers of 2D reaction-diffusion subsystems. For each layer of the system, initial conditions for spirals are appropriately applied so that a spiral is automatically generated in the layer. Spirals in different layers are coupled diffusively to form a 3D spiral wave. A 19-point approximation is used for the Laplacian operation [34] and no-flux boundary condition is applied. The above equations are integrated numerically using the Euler algorithm with the time step $dt=0.01$. For each set of parameters used in our simulations, we let the system evolve for a long enough time ($200\,000dt$) and consider only the asymptotic behaviors.

In the simulation, we chose B and f as our control parameters. The range of control parameters was set appropriately so that the system is completely in or near the excitable regime. The dissimilarities of the 2D spirals are introduced due to the gradients in the parameter B and f across the third direction. Their values increase or decrease linearly from the bottom layer (layer 1) to the top (layer 15). Other parameters are homogeneous in the system. Throughout this paper, we take the fixed parameter values: $D_u=5 \times 10^{-5}$, $D_v=3 \times 10^{-5}$, $q=2 \times 10^{-4}$, $\varepsilon=0.01$, and $A=0.08$. The values of B and f of the top layer are also fixed at $B_t=0.6$ and $f_t=1.5$.

By adjusting the values of B and f of the bottom layer B_b and f_b , the individual 2D spiral waves in the layers rotate with different frequencies and propagate with different wave speeds, which vary gradually from the bottom to the top layer. We thus generate a chain of diffusively coupled spiral rotors with dissimilarities. Without the diffusive coupling in the third direction, the 2D spirals in the 15 layers are always stable. We also found that if there is no gradient in all the parameters, 3D synchronized scroll waves are stable within the parameter range we chose. We concentrate therefore on the collective behaviors that are induced by the diffusive coupling between the 2D spirals with dissimilarity.

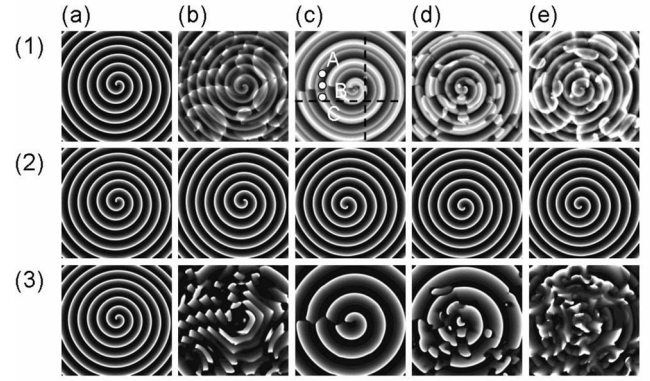


FIG. 1. Patterns of the system as the gradient in f is fixed ($f_b=2.8$) and the gradient in B is increased [columns (a)–(e)]. Snapshots in row (1) are generated by adding up the u field of the 15 layers in the third direction; those in row (2) are the snapshots taken from layer 13, and row (3) is for those in layer 5. (a) $B_b=0.6$, simple scroll wave; (b) $B_b=0.4$, turbulence in the lower layers (below layer 7), with a spiral maintained in the upper layers; (c) $B_b=0.1$, a spiral with a line defect in the lower layers, the spiral maintained in the upper layers; (d) $B_b=0.09$, state with lots of small winding pieces of line defects in the lower layers and stable spiral in the upper layers; and (e) $B_b=0.07$, turbulence again in the lower layers.

III. SIMULATION RESULT

In the first series of simulations, we keep the gradient of parameter f fixed ($f_b=2.8, f_t=1.5$) and vary the gradient in B by tuning B_b . When B is homogeneous throughout the system with $B_b=B_t=0.6$, the 2D spirals are synchronized due to the diffusive coupling [Fig. 1(a)] (the patterns are a gray-scaled map of the field for the inhibitor; white represents a high value and black a low value). All the 2D spirals oscillate at a compromised frequency as has also been observed in Ref. [16]. This state remains stable even with a gradient in B in the system, given that the gradient is small enough.

When the gradient in B becomes larger, the collective behavior of the system becomes complex. As the gradient in B is increased by decreasing B_b from 0.6 to 0.4, the integrity of the spiral wave is ruined. As a result, the system splits into two independent parts: the upper layers (from layer 8 to layer 15) are still synchronized into one 3D spiral, while the spirals in the lower layers (from layer 7 below) become unstable and turn into turbulence. Figure 1(b) demonstrates a snapshot of the 3D spiral in the upper layer [Fig. 1(b2)] and that of the turbulence state of the lower layer [Fig. 1(b3)]. We refer to this decoupled state as “partial turbulence.” We notice that within the whole parameter regimes used in our simulations, if the system has different behaviors between the upper layers and the lower layers, their boundary is around layer 7, thus snapshots of layer 5 and layer 13 are always representative of the lower part, and the upper part respectively [Fig. 1(2)(3)].

The state of partial turbulence remains stable in a range of B_b ($B_b=0.4-0.2$); but when B_b is decreased further to 0.1, another transition occurs: while the upper layers still retain the 3D spiral which is stable and intact [Fig. 1(c2)], in the lower layers, the turbulence is suppressed and the line de-

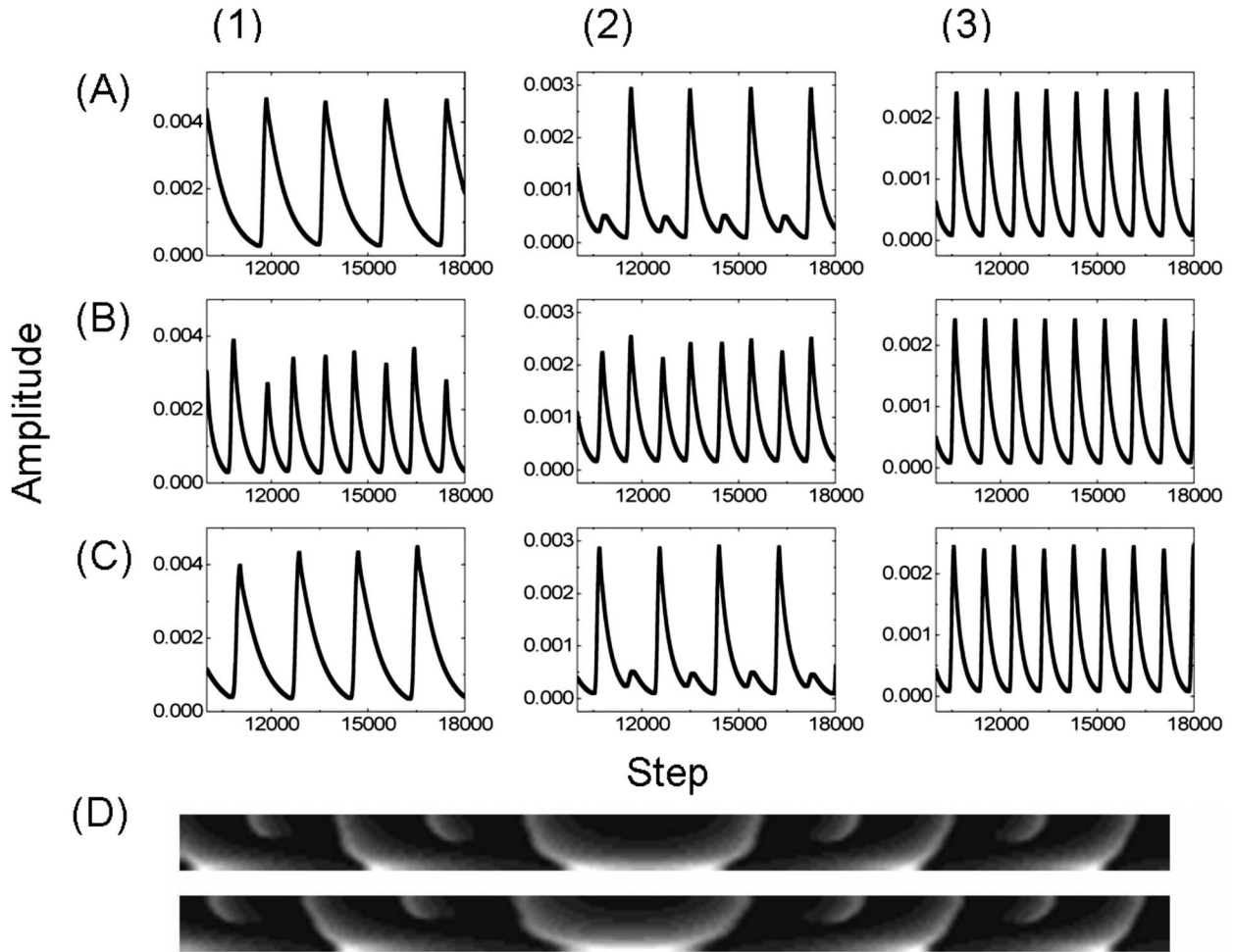


FIG. 2. Time series recorded from layer 3 (column 1), layer 7 (column 2), and layer 13 (column 3) at locations A [row (a)], B [row (b)], and C [row (c)] as marked in Fig. 1(c1). B is on the line defect with A and C its two opposite neighboring points. The bottom panel (d) displays two vertical sections of the 3D pattern from the locations marked with dashed lines in Fig. 1(c1).

fects evolve out, where two loops of periodic cycle exchange. We observed that small segments of line defects are slowly formed out of the turbulence in the lower layers. These small segments of line defects fuse together, forming longer line defects. The system eventually self-organizes into an ordered spiral wave with one or just a few (depending on the initial condition) line defects which start from the spiral tip to the boundary [Fig. 1(c3)](for the dynamic process, see the movie online [35]). A 2D projection snapshot generated from the sum of v field of the 15 layers thus gives a spiral pattern with a “line defect” [Fig. 1(c1)].

Figures 2(a)–2(c) demonstrate the time evolutions recorded from the same locations at the horizontal plane but from different layers, as marked in Fig. 1(c1) with A, B, and C. Basically, the oscillations throughout the system are of simple P-1 type. In the pattern that has been separated into two parts, the frequency of the upper layers is a fold faster than that of the lower layers, with the exception on the defect line [see row (b) in Fig. 2]. In the transition layer between the upper part and the lower part, the oscillations on the two opposite neighboring locations of the defect make a compromise between the fast oscillation of the upper part and the slower oscillation of the lower part. This comes out of the

combined oscillation profile of P-2 type oscillation [see Figs. 2(A2) and 2(C2)]. The line defect we find here is similar to previous findings of line defect observed in 2D spiral waves where the local dynamics of the media undergoes a period-doubling cascade [25–30]. In contrast to the previous findings, the line defect is obviously not a consequence of period doubling because the oscillations in the system are basically of P-1 type. The “P-2”-like oscillation is local in the system and comes out as a compromise of the fast and slow oscillations. As demonstrated clearly by the vertical sections of the 3D pattern in Fig. 2(d), the system performs P-1 type oscillations throughout the media. As the system is three-dimensional and has gradient in the third direction, we suggest that the line defect actually comes out as a result of reconciliation of the coupled spirals that have different frequencies and propagating speeds. Besides, we notice that the defect lines in different layers of the lower part of the system have exactly the same shape and direction, thus they merge into a “defect plane.”

The ordered structures shown in Fig. 1(c) are stable in a range of the control parameter B_b . However, when B_b is further decreased to 0.07, lower layers with the defect lines lose stability. They decouple from the upper layers again and turn

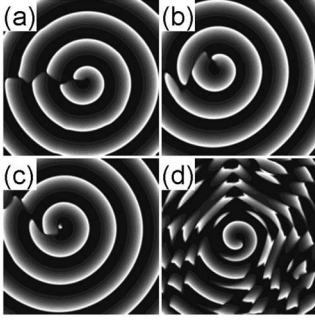


FIG. 3. Patterns of layer 5 as the gradient in f is fixed with $f_b = 2.8$ and the gradient in B is decreased by increasing B_b from 0.1 (a), to 0.12 (b), 0.13 (c), and 0.16 (d), respectively. A 3D spiral wave is sustained in the upper layers.

into line defect turbulence [Fig. 1(e3)], while the upper layers still maintain a stable 3D spiral wave [Fig. 1(e2)]. Thus the system turns into partial turbulence for a second time.

We carefully examined the transition process from the state of line defect [Fig. 1(c)] to the two states of “partial turbulence” in its neighbor regimes [Figs. 1(b) and 1(e)]. When B_b is decreased from 0.1 gradually, we observed that in lower layers, lots of small winding line defects are generated, accompanied with the original straight line breaking up into pieces. A snapshot of the system at $B_b = 0.09$ is shown in Fig. 1(d) (for the dynamic process, see the movie online [35]). However, more interesting behaviors arise when we increase B_b from the state of line defect. As demonstrated in Fig. 3 (for details see movie online [35]), when B_b is increased from 0.1, the nearly straight defect line becomes winded and sways. The line is no longer in a steady state but oscillates around its mean position. The oscillation is sinusoidal-like, with its amplitude growing as B_b is further increased. When B_b is above 0.13, the swaying becomes vehement and the shape of the defect line becomes irregular. Within the vicinity of $B_b = 0.16$, the defect lines could take various shapes, including a closed loop, a line with one end connecting to a defect and the other either to the boundary or to another defect, and lines with different angles to wave fronts (see Fig. 5). The increased irregularity of the line defects is closely associated with the increased disorder in the lower layers. The defect lines dominate the transition to turbulence as was found previously in 2D complex oscillatory media [27,30]. When B_b is further increased to 0.2, the lower layers turn into turbulence of line defects. This scenario also happens when we increase the gradient of B by decreasing B_b from the state of Fig. 1(c).

We also examined the situation when the gradient in B is fixed with $B_b = 0.1$ and the gradient in f is varied by tuning f_b . As f_b is increased from 2.8 to 3.6, the behavior is just similar to that when f_b is fixed at 2.8 and B_b is changed from 0.1 to 0.09, as shown in Fig. 1(c3) and Fig. 1(d3). On the other hand, when the gradient in f is decreased by reducing f_b from 2.8 to 1.5, the line defect becomes vibrating and various shapes of line defects show up, the process of which is the same with the case when f_b is fixed at 2.8 and B_b is increased from 0.1 to 0.13, as shown in Fig. 3. The defect lines in different layers of the lower part of the system still

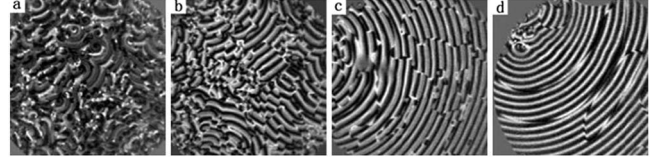


FIG. 4. Experimental snapshots with line-defected regular waves evolving out from the turbulence as the gradient in H_2SO_4 is increased [15]. Parameters: (a) $[\text{H}^+] = 0.7\text{M}$, highly disordered 3D turbulence; (b) $[\text{H}^+] = 0.8\text{M}$, wave segments with short line defects emerge; (c) $[\text{H}^+] = 0.9\text{M}$, more ordered waves with obvious line defects; and (d) $[\text{H}^+] = 1.2\text{M}$, line defects with smooth curvature.

have exactly the same shape and overlap. They merge into “defect planes,” whose location depends on initial conditions and can evolve dynamically with different parameters.

IV. COMPARISON WITH EXPERIMENT

One of the most interesting findings in our simulations is the line defect that was previously reported in 2D complex oscillatory media. We have shown that line defects can be formed as a result of reconciliation between the coupled dissimilar 2D simple spiral rotors when the system is near excitable regime, which brings the system into a more ordered state from “partial turbulence.” In fact, the process that line defect evolves out of turbulence and sequentially self-organizes into an ordered state has been found in our previous experiments, conducted in the space open reactor with a BZ reaction [15]. Figure 4 gives a typical example of such a transition. One observes that as the gradient of a control parameter ($[\text{H}_2\text{SO}_4]$) increases, the system undergoes a transition from a turbulent state to a state of ordered spiral patterns with a different type of line defects. The experimental results are in parallel with our simulations, where the patterns in the lower layers are transformed from the disordered states to ordered spiral waves with line defects [see Fig. 1(b3–c3)]. Figure 5 demonstrates the comparison of various line defects experimentally observed with those we find in our simulations with the Oregonator model. They are qualitatively in agreement.

In the Oregonator model [31,32], the dimensionless parameters q , D_u , D_v , τ , u , v , and ε are expressed as

$$q = \frac{2k_1k_4}{k_2k_3}, \quad D_u = \frac{1}{k_5B_0}D_{u0}, \quad D_v = \frac{1}{k_5B_0}D_{v0}, \quad \tau = k_5B_0t, \quad (2a)$$

$$u = \frac{2k_4}{k_3A_0}X, \quad v = \frac{2k_4k_5B_0}{(k_3A_0)^2}Z, \quad \varepsilon = \frac{k_5B_0}{k_3A_0}, \quad (2b)$$

where the rates k_2 , k_3 are proportional to $[\text{H}^+]$, k_1 is proportional to the concentration of $([\text{H}^+])^2$, and other parameters are not influenced by $[\text{H}^+]$.

By applying the rates [33], $k_1 = 2[\text{H}^+]^2\text{M}^{-3}\text{s}^{-1}$, $k_2 = 3 \times 10^6[\text{H}^+]\text{M}^{-2}\text{s}^{-1}$, $k_3 = 45[\text{H}^+]\text{M}^{-2}\text{s}^{-1}$, $k_4 = 3 \times 10^3[\text{H}^+]\text{M}^{-2}\text{s}^{-1}$, $k_5 = 1\text{M}^{-1}\text{s}^{-1}$, and $[A'] = 0.4\text{--}0.6\text{ mol/L}$, $[B'] = 0\text{--}1.2\text{ mol/L}$, $f' = 1\text{--}4\text{ mol/L}$, combined with the concentration $[\text{H}^+] = 0.4\text{--}1.5\text{ mol/L}$ applied in the experiment and $A_0 \sim 10\text{ mol/L}$, $B_0 \sim 1\text{ mol/L}$, we estimate that

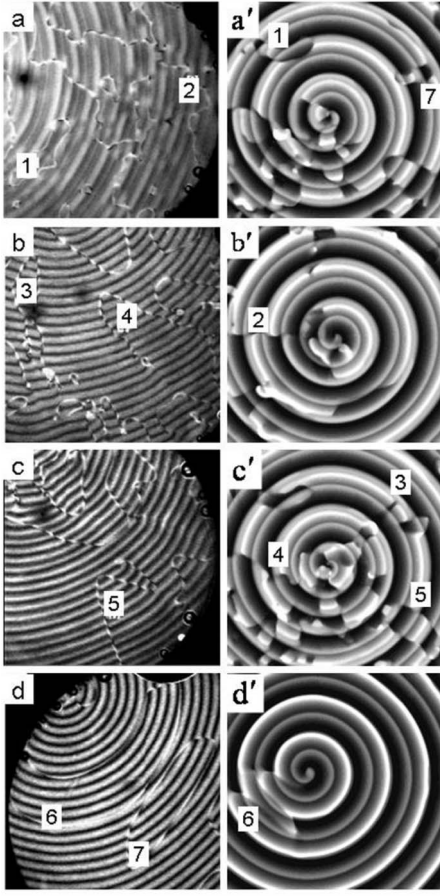


FIG. 5. Comparison of various shapes of line defect of BZ experiments [15] (left column) and simulations (right column, obtained by summing up the u field in the thin direction): 1, 7, line defects with a closed loop; 2, line defect with one end connecting to the defect and the other to the boundary; 3, line defect with both ends connecting with defects; 4, line defect with an arbitrary angle to wave fronts; 5, line defect perpendicular to wave fronts; and 6, line defect parallel to wave fronts. The simulation results are generated with B_b around 0.13 with other parameters the same as Fig. 1.

$A \sim 10^{-2}$, $B \sim 10^{-1}$, $f \sim 1$, $\varepsilon \sim 10^{-2}$, and $q \sim 10^{-4}$, which are qualitatively in accordance with the parameters we used in our simulations with Eq. (1).

From the above expressions of Eq. (2), q , D_u , D_v , and τ are not influenced by $[H^+]$. The influence of $([H^+])^2$ will be expressed through k_3 . By performing a scaling $k_3 = k_{30}k_3'$, Eqs. (1a) and (1b) are readily transformed into the following new form:

$$\frac{\partial u}{\partial(\tau k_3')} = \frac{1}{\varepsilon} \left(Au - \frac{1}{k_3'} u^2 + f \frac{B}{k_3'} v \frac{qAk_3' - u}{qAk_3' + u} \right) + D_u \nabla^2 \left(\frac{1}{k_3'} u \right), \quad (3a)$$

$$\frac{\partial v}{\partial(\tau k_3')} = Au - \frac{B}{k_3'} v + D_v \nabla^2 \left(\frac{1}{k_3'} v \right), \quad (3b)$$

where k_3' is the dimensionless form of k_3 .

The term u^2 is of second order which is smaller than other terms and its influence could be neglected most of the time. It is also reasonable to neglect the influence of k_3' on the term $\frac{qAk_3' - u}{qAk_3' + u}$. With appropriate rescaling of the time and the space, we can equal the effect of increasing k_3' to the effect of decreasing B . In this sense, the increase of $[H^+]$ in our experiment, which will enlarge the discrepancy of k_3' , would be equivalent to the decrease of B_b that we adopt in our simulations. It is thus reasonable to believe that the experimental observations of Fig. 4 can be qualitatively compared with our numerical findings of Figs. 1(b) and 1(c).

V. DISCUSSION AND CONCLUSION

We have investigated the collective behaviors of diffusively coupled 2D spiral rotors with the dissimilarity caused by multiple gradients. As the gradients and thus the difference between the coupled rotors are adjusted, the 2D spirals can be synchronized to form a 3D spiral wave, or split into two parts, one of which maintains the ordered spiral pattern, the other part forms line-defected spiral waves or line-defected turbulence. We demonstrated that the line defect, which was previously expected to be generated through a period-doubling cascade, can also form through the reconciliation between the coupled dissimilar spirals near the excitable regime. The order of the collective behaviors of the system does not monotonously depend on the changes in the gradients. As the differences between the coupled rotors are increased, ordered and disordered states alternately appear. 2D spirals with a small difference can synchronize into a 3D wave, but a part of this pattern will lose its stability and undergoes a transition into partial turbulence as their dissimilarities are increased. Ordered waves with line defect can grow out of the turbulence if one continuously increases the gradients, and the line-defected waves give way to turbulence again as the gradients are increased even further. The simulations are proven to be qualitatively comparable with those observed in 3D BZ experiments.

The complex behaviors of the coupled spirals are due to the dissimilarities among the spirals in different layers. While these phenomena are not ready for a full mathematical analysis, we can derive certain dynamic properties of the system from our simulations. By calculating the intrinsic oscillation frequency of an individual 2D spiral, we observe that the dissimilarities between the spiral frequencies grow monotonously as the gradients in B or in f are increased. Figure 6 demonstrates the frequency discrepancy with a different gradient in B [Fig. 6(a)] or in f [Fig. 6(b)]. We notice that the cascade transitions of ordered-disordered states happens in the same range of frequency differences. As can be seen in Figs. 1 and 6, the first order-disorder transition occurs as the frequency difference is around $4.1 \times 10^{-4}/\text{t.u.}$ ($B_b = 0.4$, t.u. is the abbreviation of time unit, i.e., $dt = 0.01$), while the ordered spiral with a line defect appears as the difference in frequency attains to $8.6 \times 10^{-4}/\text{t.u.}$ ($B_b = 0.1$). The second ordered-disordered transition takes place when the frequency difference is around $8.8 \times 10^{-4}/\text{t.u.}$ ($B_b = 0.09$). The same scenario also happens when we fix the gradient in B and varies the gradient in f (in this range of

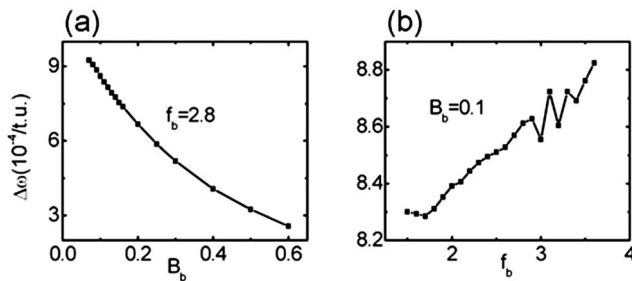


FIG. 6. Frequency discrepancy between the top and the bottom layers as the gradient in f is fixed and that in B is reduced (a), or gradient in B is fixed and that in f is increased (b).

parameter the frequency difference cannot be reached to $3.5 \times 10^{-4}/\text{t.u.}$, the onset of the first order-disordered transition). These observations imply that the behavior of the system essentially depends on the gradient of intrinsic frequency (i.e., $\Delta\omega$ in Fig. 6), rather than on the gradient of any particular parameter. We thus suggest that the frequency discrepancy ($\Delta\omega$) is probably the essential factor determining the behavior of the system. When $\Delta\omega$ is small, the 2D spirals can be synchronized into a whole to form a 3D spiral. Once

$\Delta\omega$ grows across a threshold, the integrity will be ruined and the system decouples into two parts, one of which can further transit into turbulence. Nevertheless, when $\Delta\omega$ is further increased, the system might have fallen into certain internal frequency locking of 1:2, where the upper layers are united into a uniform P-1 oscillation whose frequency is a fold faster than the lower part except on the line defect. At this time, the rotors in the lower layers will have to go along with line defects due to their frequency conflicts and subsequent reconciliations. Even larger $\Delta\omega$ will again destroy the resonance and the system turns into partial turbulence again. This coupling scenario may generally exist in many diffusively coupled spatiotemporal patterns.

ACKNOWLEDGMENTS

This work was supported by the NSF of China (Grant No. 10774008) and the National Basic Research Program of China (Grants No. 2006CB910706 and No. 2007CB814800). C.W. and X.L. thank the National Foundation for Fostering Talents of Basic Science (Grant No. J0630311) and Jun-Zheng Foundation at Peking University for support.

-
- [1] D. C. Michaels, E. P. Matyas, and J. Jalife, *Circ. Res.* **61**, 704 (1987).
- [2] J. Aldridge and E. K. Pye, *Nature (London)* **259**, 670 (1976).
- [3] J. Buck, *Q. Rev. Biol.* **63**, 265 (1988).
- [4] T. J. Walker, *Science* **166**, 891 (1969).
- [5] K. Wiesenfeld, P. Colet, and S. H. Strogatz, *Phys. Rev. E* **57**, 1563 (1998).
- [6] I. Z. Kiss, Y. Zhai, and J. L. Hudson, *Science* **296**, 1676 (2002).
- [7] Z. Jiang and M. McCall, *J. Opt. Soc. Am.* **10**, 155 (1993).
- [8] N. Wiener, *Nonlinear Problems in Random Theory* (MIT Press, Cambridge, MA, 1958); *Cybernetics* (MIT Press, Cambridge, MA, 1961).
- [9] A. T. Winfree, *J. Theor. Biol.* **16**, 15 (1967).
- [10] Y. Kuramoto, *Chemical Oscillations, Waves, and Turbulence* (Springer, Berlin, 1984).
- [11] S. H. Strogatz, *Physica D* **143**, 1 (2000).
- [12] S.-J. Baek and E. Ott, *Phys. Rev. E* **69**, 066210 (2004).
- [13] J. G. Restrepo, E. Ott, and B. R. Hunt, *Phys. Rev. Lett.* **96**, 254103 (2006).
- [14] H. Guo, L. Li, H. Wang, and Q. Ouyang, *Phys. Rev. E* **69**, 056203 (2004).
- [15] C. Zhang, H. Liao, and Q. Ouyang, *J. Phys. Chem. B* **110**, 7508 (2006).
- [16] C. Wang, S. Wang, C. Zhang, and Q. Ouyang, *Phys. Rev. E* **72**, 066207 (2005).
- [17] A. V. Panfilov and A. N. Rudenko, *Physica D* **28**, 215 (1987).
- [18] P. K. Brazhnik, V. A. Davydov, V. S. Zykov, and A. S. Mikhailov, *Sov. Phys. JETP* **66**, 984 (1987).
- [19] V. N. Biktashev, A. V. Holden, and H. Zhang, *Philos. Trans. R. Soc. London, Ser. A* **347**, 611 (1994).
- [20] H. Henry and V. Hakim, *Phys. Rev. Lett.* **85**, 5328 (2000).
- [21] S. Alonso, F. Sagues, and A. S. Mikhailov, *Science* **299**, 1722 (2003).
- [22] Y. Wu, C. Qiao, Q. Ouyang, and H. L. Wang, *Phys. Rev. E* **77**, 036226 (2008).
- [23] X. Lu, C. Wang, C. Qiao, Y. Wu, Q. Ouyang, and H. Wang, *J. Chem. Phys.* **128**, 114505 (2008).
- [24] M. Yoneyama, A. Fujii, and S. Maeda, *J. Am. Chem. Soc.* **117**, 8188 (1995).
- [25] J. S. Park and K. J. Lee, *Phys. Rev. E* **73**, 066219 (2006).
- [26] J. S. Park and K. J. Lee, *Phys. Rev. Lett.* **88**, 224501 (2002).
- [27] J. S. Park and K. J. Lee, *Phys. Rev. Lett.* **83**, 5393 (1999).
- [28] A. Goryachev and R. Kapral, *Phys. Rev. E* **54**, 5469 (1996).
- [29] A. Goryachev, H. Chate, and R. Kapral, *Phys. Rev. Lett.* **80**, 873 (1998).
- [30] A. Goryachev, H. Chate, and R. Kapral, *Phys. Rev. Lett.* **83**, 1878 (1999).
- [31] J. J. Tyson and P. C. Fife, *J. Chem. Phys.* **73**, 2224 (1980).
- [32] D. A. Vasquez, W. Horsthemke, and P. McCarty, *J. Chem. Phys.* **94**, 3829 (1991).
- [33] R. J. Field and H.-D. Försterling, *J. Phys. Chem.* **90**, 5400 (1986).
- [34] M. Dole, R. M. Mantel, and D. Barkley, *Int. J. Bifurcation Chaos Appl. Sci. Eng.* **7**, 2529 (1997).
- [35] See EPAPS Document No. E-PLLEE8-79-135901 for movies corresponding to Figs. 1 and 3. For more information on EPAPS, see <http://www.aip.org/pubservs/epaps.html>.